Long-term, genome-wide kinetic analysis of the effect of the circadian clock and transcription on the repair of cisplatin-DNA adducts in the mouse liver

Received for publication, May 30, 2019, and in revised form, June 19, 2019 Published, Papers in Press, June 19, 2019, DOI 10.1074/jbc.RA119.009579

Yanyan Yang, Zhenxing Liu, Christopher P. Selby, and Aziz Sancar[1]

From the Department of Biochemistry and Biophysics, School of Medicine, University of North Carolina at Chapel Hill, Chapel Hill, North Carolina 27599

Edited by Patrick Sung

Cisplatin is the most commonly used chemotherapeutic drug for managing solid tumors. However, toxicity and the innate or acquired resistance of cancer cells to the drug limit its usefulness. Cisplatin kills cells by forming cisplatin-DNA adducts, most commonly the Pt-d(GpG) diadduct. We recently showed that, in mice, repair of this adduct 2 h following injection is controlled by two circadian programs. 1) The circadian clock controls transcription of 2000 genes in liver and, via transcription-directed repair, controls repair of the transcribed strand (TS) of these genes in a rhythmic fashion unique to each gene's phase of transcription. 2) The excision repair activity itself is controlled by the circadian clock with a single phase at which the repair of the nontranscribed strand (NTS) and the rest of the genome takes place. Here, we followed the repair kinetic for long periods genome-wide both globally and at single nucleotide resolution by the Excision Repair-sequencing (XR-seq) method to better understand cisplatin DNA damage and repair. We find that transcription-driven repair is nearly complete after 2 days, whereas weeks are required for repair of the NTS and the rest of the genome. TS repair oscillates in rhythmically expressed genes up to 2 days post injection, and in all expressed genes, we see a trend in TS repair with time from the 5′ to 3′ end. These findings help to understand the circadian- and transcription-dependent and -independent control of repair in response to cisplatin, and should aid in designing cisplatin chemotherapy regimens with improved therapeutic indexes.

Circadian rhythmicity of metabolic processes significantly impacts physiology and behavior (1). As a notable example, in mice, excision repair of DNA damage is rhythmic, and daily variations in repair activity are associated with daily variations in sensitivity to UV-induced skin cancer (2, 3). The molecular basis for the circadian clock is a transcription-translation feedback loop in which transcription of clock-controlled genes is activated by BMAL1-CLOCK heterodimers binding to E-box elements in their promoters. *Crys* (*Cry1* and *Cry2*) and *Pers* (*Per1* and *Per2*) are clock-controlled, core clock genes and PER and CRY proteins inhibit BMAL1-CLOCK and rhythmically repress transcription of their own and other clock-controlled genes. The processes of CRY and PER protein degradation, synthesis, and nuclear transport contribute to the 24-h periodicity of this loop. Secondary transcriptional feedback control loops stabilize the clock, and different circadian-controlled genes have different sets of regulatory elements that fine-tune their expression in a tissue- and time of day–specific manner (1).

Chronotherapy, the timed administration of drugs, takes advantage of circadian variations in therapeutic ratio exhibited by some drugs. It is possible that platinating anticancer drugs exhibit circadian variations in therapeutic ratio because these drugs kill cells by binding to DNA, excision repair is the sole mechanism for repairing platinated DNA (4–6), and excision repair of DNA is controlled by the circadian clock. To investigate this possibility, we have been using the XR-seq[2] method (7–9) which allows us to map, across an entire genome, at single nucleotide resolution, where excision repair has occurred among a population of cells. We have applied this method to cells of different organisms (10–12), and recently we adapted XR-seq to mice, where we found two main circadian programs of repair (13, 14). First, basal nucleotide excision repair activity exhibits a single peak at about ZT 8–10 (ZT = 0 is time of lights on and ZT = 12 is lights off under 12 h light:12 h dark conditions) which is associated with a corresponding rhythmic oscillation of the XPA excision repair factor (2, 3). This program controls repair of the nontranscribed strand (NTS) of genes, weakly and nontranscribed genes, and intergenic regions. In addition to the basal repair pathway is a highly efficient transcription-coupled excision repair pathway which utilizes basal repair proteins to remove transcription-blocking lesions from the transcribed/template strand (TS) of active genes (15). In constitutively expressed genes, TS repair is greater than NTS repair, and the relative TS repair of a given gene reflects its transcription activity. Interestingly, circadian-controlled genes exhibit peak and trough TS repair levels that occur at times of day specific to each gene, although most rhythmic genes exhibit

This work was supported by National Institutes of Health Grants GM118102 and ES027255 (to A. S.). The authors declare that they have no conflicts of interest with the contents of this article. The content is solely the responsibility of the authors and does not necessarily represent the official views of the National Institutes of Health.

The raw data and alignment data have been deposited in the Gene Expression Omnibus under accession numbers GSE132002 and GSE132993.

[1] To whom correspondence should be addressed. E-mail: aziz_sancar@med.unc.edu.

[2] The abbreviations used are: XR-seq, Excision Repair-sequencing; NTS, nontranscribed strand; TS, transcribed/template strand; RNAP, RNA polymerase; TSS, transcription start site; TCR, transcription-coupled repair; ssDNA, single-stranded DNA; RPKM, reads per kilobase pairs per million; ZT, zeitgeber time; TES, transcription end site; Pt, platinum.

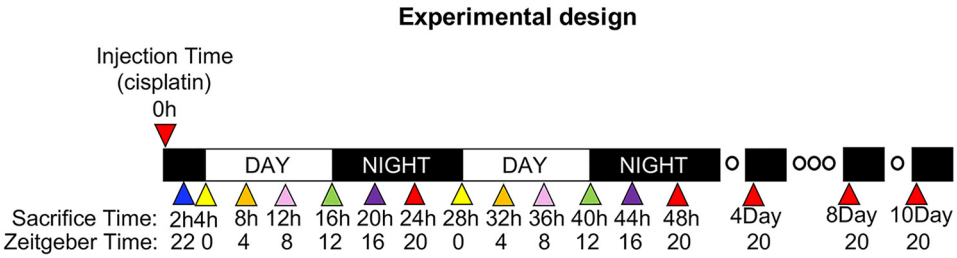

Figure 1. Experimental design. Cisplatin was injected intraperitoneally at ZT20 (3:00 a.m.) and at the indicated times (hours post injection and ZT) mice were sacrificed and livers were harvested for Pt-d(GpG) adduct level measurements and high-resolution genomic repair mapping. For the first 2 days sampling was done every 4 h except the first time point (2 h after injection). Thereafter sampling was done 4, 8, and 10 days after injection as indicated, and at 5-day intervals thereafter until day 70 (not shown). *Triangle* colors represent different zeitgeber times: ZT0, *yellow*; ZT4, *orange*; ZT8, *pink*; ZT12, *green*; ZT16, *purple*; ZT20, *red*; ZT22, *blue*.

a peak around pre-dawn or pre-dusk (1). In this repair program, each gene-specific repair pattern parallels the corresponding gene-specific circadian transcription pattern as determined by methods such as NET-seq and GRO-seq (16–18). Interestingly, as a consequence of these two circadian programs, in many circadian genes the peak and trough repair times are different for the TS and NTS. The data in this study were obtained by injecting cisplatin at 4-h intervals over the course of a day, and sampling liver 2 h after each injection. Although useful, this setup does not replicate or characterize the clinical treatment scenario.

In clinical oncology, cisplatin is given repeatedly, at 1- to 2-week intervals to allow the patient to recover from side effects before the following dose (19–22). With this consideration, then, we decided to investigate the repair patterns and kinetics of cisplatin damage in mouse liver for a period of 70 days following a single dose, using both slot blot to measure total repair trend and XR-seq to obtain a high-resolution dynamic map of repair and to understand how the two parameters, circadian clock and transcription, affect the repair pattern over the course of days following drug administration. Interestingly, we observe transcription-driven, rhythmic repair in the TS for 2 days post-injection, indicating that the circadian clock (transcription-translation feedback loop) persists following DNA damage. We also observe a clock-independent progression of TS repair, with time, from the 5′ to the 3′ end of genes. Transcription-coupled repair is complete by about 2 days, at which point repair of the NTS and the remainder of the genome becomes dominant and persists until it approaches the limit of detection at 70 days.

Results

To follow the Pt-d(GpG) repair pattern over a 10-day period, 59 mice were injected with cisplatin (10 mg/kg) at ZT20 (3:00 a.m.) on day 1 (Fig. 1), and for the first 2 days afterward 3 mice were sacrificed at 4-h intervals, their livers were harvested, and Pt-d(GpG) repair was quantified by slot blot and XR-seq. For the remaining mice, 6 to 8 per time point were sacrificed at 4, 8, and 10 days after cisplatin injection and were processed likewise. An additional 12 mice were injected with cisplatin on day 1, as above, and livers were harvested for slot blot analysis at 5-day intervals from day 15 to day 70. Insufficient material was available for XR-seq analysis of samples obtained later than 10 days after injection.

A fairly comprehensive view of repair can be obtained by using the slot blot and XR-seq methods together (9). The slot blot method measures the total amount of damage throughout the genome using an anti–Pt-d(GpG)-DNA antibody. Loss of immunoreactivity in DNA with time is an indirect measure of repair. In XR-seq, Pt-adducted DNA, removed from the genome by excision repair in the form of predominantly 26 to 27 base oligonucleotides, is purified from tissues at various times after injection. These excision products are processed for next generation sequencing, and the sequences are mapped to the genome to identify where repair has occurred. Of note, the excision products are degraded within cells at the same time they are generated. Therefore, whereas the slot blot measures cumulative repair with time, XR-seq provides a "snapshot" of where repair has occurred at the time of sampling.

Overall genome repair kinetics

Slot blot analysis of total damage and repair in liver is shown in Fig. 2. The data show that adducts reach their highest level 2 h after injection. Importantly, after a relatively rapid repair rate, repair proceeds at a slower rate from about 2 days on until adduct levels reach the limit of detectability at 30 to 70 days in agreement with previous studies using the same mAb for quantifying cisplatin adducts by immunostaining (23).

Genome-wide repair kinetics at single nucleotide resolution

The analysis of total genomic repair, although informative, does not provide insight about the potential significance of the early and late repaired regions and the effect of differential gene expression on repair and survival. XR-seq, which reveals repair genome-wide and at single nucleotide resolution, is ideally suited for this purpose. Fig. 3 shows XR-seq data from 2 h to 10 days for three constitutively expressed genes, a housekeeping gene (*Dhfr*), a gene adjacent to *Dhfr* but transcribed in the opposite direction, the mismatch repair gene *Msh3*, and the checkpoint gene *Atr*. Shown in Fig. 4 are the XR-seq data for two rhythmic genes, the circadian clock gene *Npas2* and the clock-controlled gene *Dpb* (1). The screenshots in Figs. 3 and 4 show the distribution of repair across each of these genes at selected times, and the graphs plot quantitative levels of TS and NTS repair for each gene as a function of repair time. Several points emerge from this figure. First, for the constitutively expressed *Msh3*, *Dhfr*, and *Atr*, TS repair strongly dominates over NTS repair for the first 8 h following injection. Only after

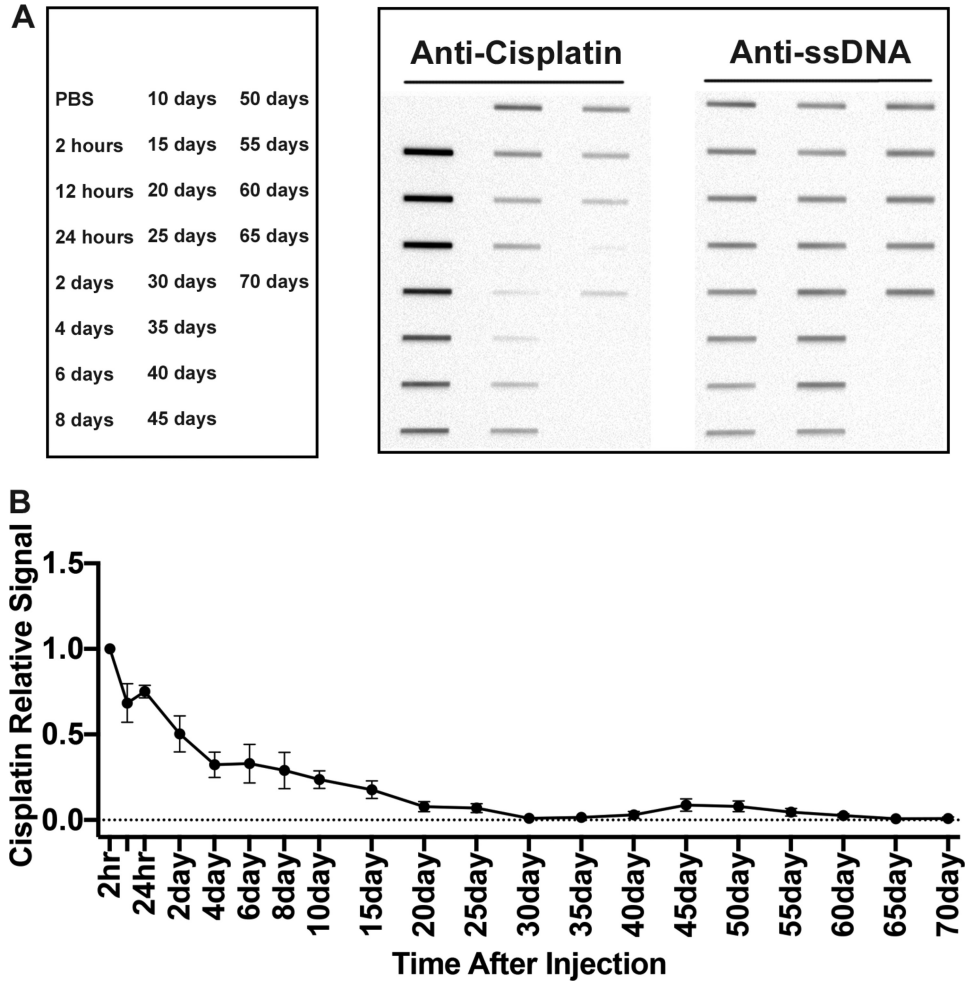

Figure 2. Overall Pt-d(GpG) adduct removal from the genome. Cisplatin was injected into three mice per time point. Following cisplatin injection at the indicated time points, DNA was isolated from liver and the Pt-d(GpG) adduct levels were estimated by slot blot. *A*, *left panel*, schematic of time points. *Right panel*, slot blot for Pt-d(GpG), and slot blot for ssDNA of the samples assayed for Pt-d(GpG). *B*, *bottom panel*, quantitative analysis of data of *top panel's* right and a technical replicate. *Error bars* indicate S.E. *PBS*, no drug control.

24 to 48 h does NTS repair approach the level of TS repair in these three genes. This is because at early time points the TS repair, which proceeds at a faster rate (15), depletes most of the damage in the TS such that at later time points the amount of damage in the TS is so low that the repair of the remaining adducts by TCR is comparable with the repair of NTS adducts which remain at a high level. Eventually the TS is depleted of damage by the efficient coupled repair pathway so that after 48 h, global repair of the NTS predominates in these genes. Interestingly, there appears to be a modest TS repair peak in these genes at approximately 24 to 36 hours post-injection (Fig. 3). These modest peaks may reflect oscillation in basal repair superimposed upon the much stronger TCR signal.

Compared with the constitutively expressed genes, the repair patterns seen in the TS of the rhythmic *Npas2* and *Dbp* genes (Fig. 4) are quite striking. The constitutively expressed genes exhibit peaks in TS repair shortly following injection that gradually decrease. In contrast, TS repair in *Npas2* abruptly decreases to the NTS level by 12 h post injection (ZT8). This relatively abrupt decrease reflects two processes. First is the abrupt inhibition of *Npas2* transcription, which exhibits a nadir at ZT6 to ZT18 and a peak at ZT22 (16). Secondly, during each round of transcription-coupled repair, the polymerase blocked by the adduct is removed from the template (24–27). Thus, by 12 to 20 h post injection, transcription initiation is stopped by the clock, and polymerases having engaged in transcription-coupled repair are dissociated, leaving the template polymerase-free. However, TS repair of the *Npas2* gene is incomplete at 20 h, as multiple lesions per TS in long genes are expected, based upon estimates of one Pt adduct per 4000 bp in liver under the treatment condition we used (23). Thus, when the clock initiates a new wave of *Npas2* transcription at ~24 h post injection (ZT20), there is an associated transcription-coupled TS repair peak at 24 to 28 h. A following wave of transcription-coupled repair peaking at 48 h completes TS repair, and thereafter, NTS repair dominates. Other large genes also demonstrate two waves of transcription-coupled repair. However, here we wished to demonstrate the effect of transcription phase in repair pattern by choosing *Dbp* (Fig. 4), which is transcribed anti-phase to *Npas2*. As seen in Fig. 4, *bottom*, in contrast to *Npas2*, the first TS repair peak of *Dbp* is at ZT08 (10 h separated from the ZT22 peak of *Npas2*) (16). The second *Dbp* TS repair peak is barely discernible because in this small gene, by the second circadian cycle most of the TS repair is complete.

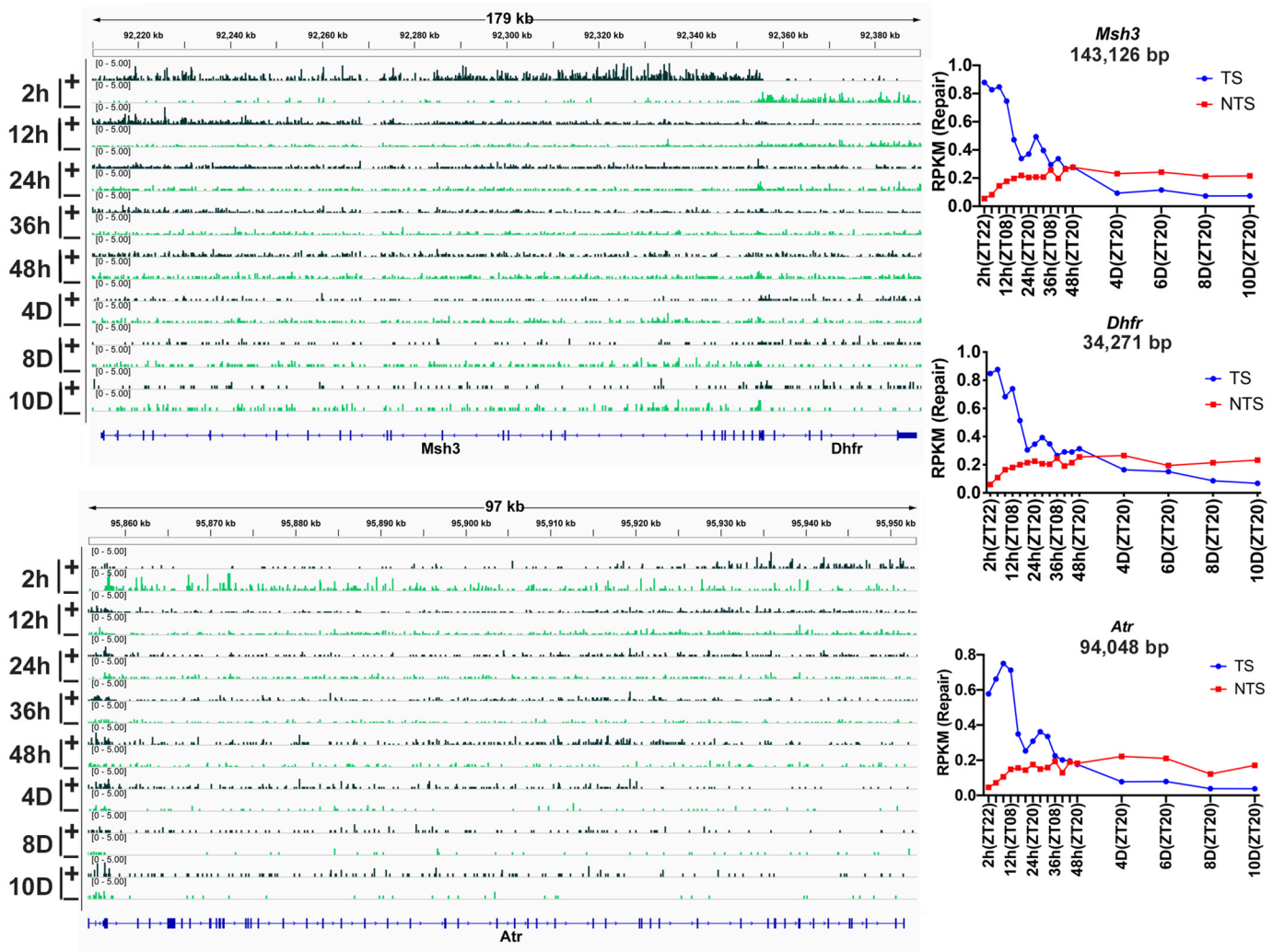

Figure 3. XR-seq analysis of repair in constitutively expressed genes. Screenshots illustrate the distribution of repair across the two strands of select genes at different times following injection of cisplatin at ZT20 (0 h). The screenshots show repair in three highly transcribed housekeeping genes that are transcribed in different directions. For *Msh3*, the (+) strand; *Dhfr*, the (−) strand; and for *Atr* the (−) strand is the transcribed strand (TS). Plus strand repair is in *black* and minus strand is in *green*. Plots to the right of each panel illustrate quantitative values for repair of the TS and NTS for each gene at select time points. Note that although at early time points the TS repair dominates for the housekeeping genes, thereafter, TS repair gradually decreases and by 48 h, the NTS becomes the main source of repair products because of the depletion of damage in the TS as a consequence of highly efficient TCR. NTS and TS repair levels are plotted as number of repair reads per thousand bp per million mapped reads (RPKM).

Polarity of cisplatin repair in mouse genes

An earlier XR-seq kinetic study in yeast demonstrated a trend in progression of TS repair from the 5′ to the 3′ end with time. This scenario is consistent with an underlying process of repetitive cycles of removal of RNAP from the template with each repair event followed by transcription initiation at the promoter and then blockage and repair as adducts are successively removed in the 5′ to 3′ direction (26–31). We analyzed our data to see if such a polarity existed in mice by plotting, at each time point, the average repair distribution in the TS of transcriptionally active genes. Genes over 100 kbp in length which are more likely to have multiple damages per TS were used in the analysis (32). The results in Fig. 5 do in fact show polarity in repair as a trend. Starting at the earliest (2 h) time point, gene-wide, there is greater repair toward the 5′ end compared with the 3′ end, that is, the TS repair level slopes downward across the unit gene body. Thereafter, with time, there is a concurrent decrease in TS repair at the 5′ end, and increase toward the 3′ end. Also, with the time, the overall repair level of the TS decreases (note the *y* axis scale at each time) as TS repair nears completion and repair shifts to other regions of the genome. In contrast to the polarity exhibited by the TS, after 48 h NTS repair rather uniformly increases from an initial low level, and after 48 h the NTS repair becomes predominant over TS repair.

Among the factors contributing to polarity in TS repair is the high density of RNAPII normally present at the promoter region and immediately downstream (8, 33–35). Evidence for this population in our data is seen as a strong peak in repair near the transcription start site (TSS) in Fig. 5; this peak has been commonly observed in XR-seq studies. Thus, when Pt-DNA adducts are formed, polymerases at the promoter and the less densely populated gene body elongate, become blocked, mediate coupled repair (with more repair events near the promoter), and are released. Thereafter, in succession, newly initiating polymerases engage in coupled repair and are released (29–31), so that damage at the 3′ end is repaired last.

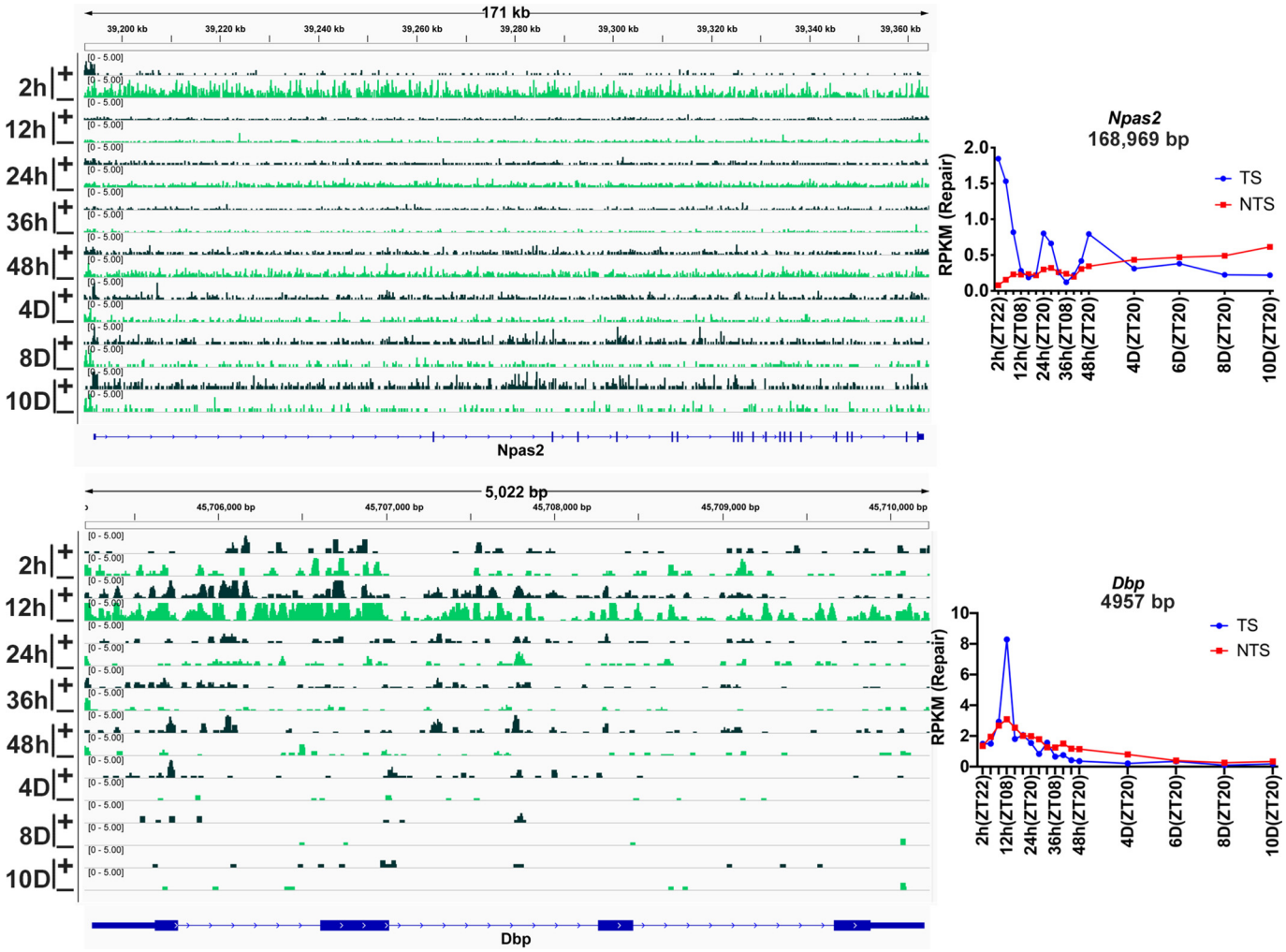

Figure 4. XR-seq analysis of repair in circadian-controlled genes. The screenshots show repair profiles for two circadian-controlled genes, *Npas2*, which has a peak expression at ZT22, and *Dbp*, which peaks at ZT10. Plots to the right of each panel illustrate quantitative values for repair of the TS and NTS for each gene at select time points. Repair in the rhythmic *Npas2* exhibits high amplitude TS (−) strand repair peaks at 2 h, ~24 h, and ~48 h after drug injection. Only after 48 h does the NTS becomes the main source of repair product from *Npas2*. In the clock-controlled *Dbp* gene, the TS (−) strand repair exhibits peaks at ~12 h and ~32 h after drug injection.

The NTS also exhibits a peak in repair near the TSS, but the NTS exhibits no polarity in repair. This peak, commonly observed in XR-seq studies, results from antisense transcription (8, 33–35) which progresses away from the gene body. The NTS is primarily repaired by the global repair program.

Interestingly, the polarity in repair reported here was seen at only modest levels in XR-seq studies of repair of UV and cisplatin damage in cultured human cells (8, 33). This is because of several factors. Among these, mouse tissues exhibit relatively strong, readily detected transcription coupled repair. Also, we focused our analysis on long genes, to enrich in genes with multiple adducts per TS. Notably, the polarity was absent when genes from our dataset 10 kbp and shorter were analyzed.

TS and global repair kinetics

To quantitatively compare the levels of transcription-dependent and -independent repair in liver, we analyzed separately the fraction of repair originating from the TS of genes, and the fraction originating from the remainder of the genome (*i.e.* the NTS of genes and intergenic DNA). Results are shown in Fig. 6. Although the TS constitutes a small fraction (about 16%) of the genome, in the first 2 h following drug injection about 70% of repair in liver is in the TS of active genes. Only after 8 h do the contributions of the two modes of repair intersect, and the non-transcribed/intergenic repair gradually becomes the dominant form such that by 10 days post injection it constitutes about 80% of the repair products. The expectation is that because transcription-coupled repair is nearly complete after 48 h, the contribution of TS repair to total repair at 48 h would be close to or below the value of 16%, the approximate percent of the genome that is TS. Many of the genes included in the analysis are in fact not or weakly transcribed, and repair of the TS of these genes by the global repair pathway would make the overall value of %TS repair closer to 16%, whereas more complete TS repair would make the %TS repair less than 16%. On the other hand, to the extent that repair products from repetitive sequences cannot be annotated, the genome size is effectively reduced and the effective percent of the genome that is TS is

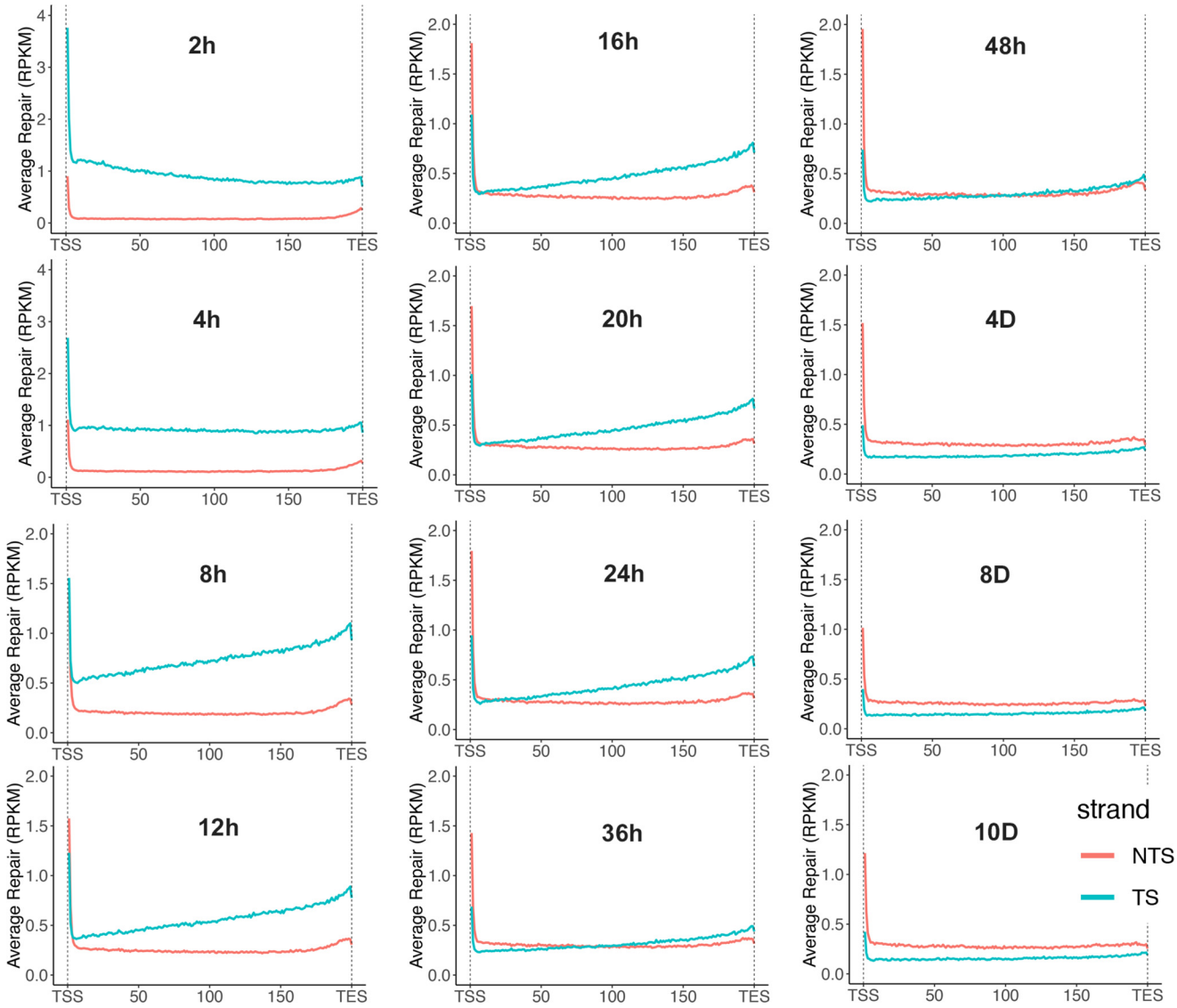

Figure 5. Polarity in repair of the TS of expressed genes. At each time point a graph plots average repair reads as average RPKM (*y* axis) along the length of a "unit gene" representing all transcribed genes longer than 100 kbp (*x* axis). The unit gene is 200 bins in length, and values for average repair were obtained by dividing each of the >100 kpb active genes into 200 bins and averaging the repair values for each successive bin from 1 to 200. The downward sloping *blue line* (TS repair) across the unit gene body at 2 h indicates more repair toward the 5′ end. Thereafter, the TS repair line flattens (4 h) and then slopes upward starting at 8 h, indicating more repair at the 3′ end. After 4 h, overall TS repair decreases (note *y* axis scales) and after 8 h it slowly flattens. By 48 h, TS repair lacks polarity and continues to decrease, in contrast to NTS repair which increases without polarity. Interestingly, RNAPII is known to be present at high concentration in the promoter region, and this leads to peaks in both sense strand and antisense strand transcription-coupled repair near the TSS (8, 33–35). Also contributing to these repair peaks, there is an ~2-fold increased level of cisplatin damage in the promoter region because of an increased concentration of the GpG sequence, which is the primary target of cisplatin. Similarly, a dip in repair near the transcription end site (TES) is associated with fewer Pt adducts and fewer GpG sequences (8).

increased. Thus, the observed value of about 20% is reasonably close to expectation.

In this study, it was not possible to monitor basal repair rhythmicity as done previously. In our prior study, the basal repair rhythmicity was not large, but it was detected among mice which were sampled 2 h after each injection (13). In the present study, with sampling of mice for increasing periods following injection, and also with the transition in repair from TS to NTS with time, significant increases in the NTS and global repair signals were produced to the extent that they dwarfed and rendered undetectable any expected circadian variations in global repair from one ZT to the next. We note that modest peaks in TS repair, evident in the data for *Msh3*, *Dhfr*, and *Atr* (Fig. 3), are suggestive of global repair rhythmicity.

Discussion

This work was undertaken to understand the repair of cisplatin-DNA adducts under conditions approximating the clinical setting and thus to help improve the optimal drug delivery regimen. Our results have, in fact, helped address this issue as well as certain questions related to circadian and transcriptional control of nucleotide excision repair in mammalian organisms.

First, our data, obtained by slot blot with anti–cisplatin-d(GpG) antibodies, showed that it takes 4–5 weeks for complete removal of Pt-DNA adducts from the genome which is in agreement with a previous report on Pt-DNA adduct repair as probed by immunostaining (23). However, high-resolution mapping by XR-seq shows that for genes transcribed with moderate to high efficiency, TS repair is 90% complete for most

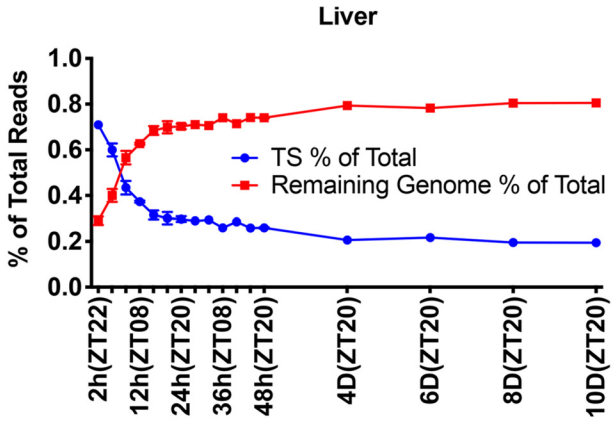

Figure 6. Genome-level analysis of the contributions of TS repair and genomic repair as a function of time after cisplatin injection. For the first ~8 h, TS repair dominates, thereafter global genomic repair becomes predominant and continues for at least 10 days.

genes in 48 h and virtually complete in 10 days. This finding may have some practical consequences: For normal nonproliferating tissues the transcription-blocking harmful cisplatin lesions are essentially eliminated in 48 h whereas the damage in the NTS remains for much longer time. Although these adducts in the NTS may be harmless for nonreplicating tissues, they have the potential to cause cell death of proliferating tumor cells by causing replication fork catastrophe and apoptosis. Naturally, these harmful effects will also impact proliferating normal tissues (skin, alimentary tract, bone marrow) but with judicial dosing regimens this negative impact can be minimized (36, 37).

Second, our data reveal an interesting aspect of the circadian clock on repair: As reported previously (13), the circadian clock controls excision repair of the TS of clock-controlled genes through its effect on transcription, and the magnitude of this effect is proportional to the transcription rate. In addition, the clock also controls the basal excision repair activity through its control of XPA expression, which peaks at ZT8–10 (2, 3). This is responsible for the peak excision repair of NTS of all genes and of both strands of all nontranscribed genes. The effect of transcription on repair of the TS is so strong that the more modest effect of repair oscillation on TS repair makes only a minor ripple which is undetectable in the genome-wide analysis of repair profiles (13). In the present study, we inspected the repair profile of genes that are >100 kbp and highly expressed at the single gene level to gain a more detailed view of the clock-transcription joint effect on repair. For clock-controlled genes such as *Npas2*, the TS repair, which is at its zenith at 2 h after cisplatin injection at ZT20 (because transcription of Npas2 peaks at ZT22), drops precipitously to the NTS level within 10 h after cisplatin injection because, as dictated by the clock, transcription is at its nadir at this time point (16). However, as expected for a clock-controlled gene, a second and third wave of transcription cycles 24 h apart produce new peaks of TS repair relative to NTS repair. After the third circadian cycle, the repair of the TS is nearly complete such that for the remaining time the NTS repair becomes dominant.

Interestingly, even though at the genome level of analysis, we could not observe the effect of the global repair activity oscillation (peak at ZT8–10) on the TS when we analyzed individual noncircadian genes of relatively large sizes (~40 kbp–150 kbp), we did observe minor circadian peaks superimposed on the major TS repair signal for one to two cycles that are mostly likely caused by the effect of repair oscillation on TS repair in these transcriptionally nonoscillating genes. Indeed, in comparing *Npas2* TS repair oscillatory peaks with those of noncircadian *Msh3*, *Dhfr*, and *Atr*, it is apparent that whereas the TS repair of *Npas2* goes below that of NTS because of transcriptional shut-off at the end of the first circadian cycle after cisplatin injection, for the nonoscillating genes TS repair always remains above the NTS until 48 h post cisplatin injection when depletion of damage of the TS results in NTS' becoming the major source of repair after this time point.

Third, analysis of TS and NTS repair of 1418 genes of size >100 kbp so as to have sufficient damage within the transcription unit enabled us to address a long-standing question in the field of mammalian transcription-coupled repair (TCR): The fate of RNAPII following TCR at the first encounter with damage in the transcribed strand. The following models have been proposed: RNAPII backs up from the damage site to allow repair without releasing the transcript and following repair it continues to elongate the uninterrupted transcript (15, 38); it remains bound at the damage site, allowing repair to take place (39–42) whereas repair elsewhere is inhibited by chromatin structure (43); it may recruit Cockayne syndrome group B protein which assists the excision repair complex to assemble rapidly without Xeroderma pigmentosum, complementation group C protein (44–46) and carry out the dual incision upon addition of Cockayne syndrome group A protein (47), following which RNAPII along with the truncated transcript may be dissociated or be ubiquitylated and degraded (24–27, 48).

We find that time course analysis of repair patterns of these >100 kbp genes reveals an interesting pattern: At early time points (0–2 h), repair is dominated by TS repair and the TS repair exhibits a 5′ to 3′ downward slope. At 4 h post damage, the TS repair profile is flat, meaning the 5′ and 3′ halves are repaired with equal efficiencies but still much more efficiently than the NTS. From 8–24 h the 3′ side of the genes becomes the predominant repair region of the TS while maintaining the preferential repair over the NTS. By 36–48 h, the TS and NTS repair are about equal and at the same level throughout the gene. By day 4 following cisplatin administration, the NTS repair becomes the predominant repair mode because by this time the TS is largely depleted of damage. We believe these data are consistent with and in support of the model positing that stalled RNAPII initiates TCR at the damage site, and concomitant with or following the repair reaction it is discarded along with the truncated RNA (26–31). Whether the RNAPII is degraded or not we cannot tell. All other models that predict continuation of the original transcript following removal of the blocking lesion are not consistent with the observation of the repair gradients with opposite slopes we observe as a function of time of repair of the TS.

Finally, from a clinical standpoint, we wish to point to the following. The total analysis of cisplatin repair in the TS *versus* rest of genome (NTS, both strands of nontranscribed genes, intergenic regions, rDNA genes) reveals that although for the

first 48 h following drug injection TS repair dominates, after that the transcription-independent repair becomes the dominant form of repair, and this fact should be considered in various strategies of assessing cisplatin treatment or the development and application of novel platinum-based drugs.

Experimental procedures

Mice

WT C57Bl/6J female mice age 3 to 6 months were used. They were purchased from The Jackson Laboratory or bred in house and were maintained in a 12-h light, 12-h dark environment and fed *ad libitum*. Mice were used according to guidelines of the National Institutes of Health and studies were approved by the Institutional Animal Care and Use Committee at the University of North Carolina at Chapel Hill.

Cisplatin at 1 mg/ml with NaCl at 9 mg/ml was from Fresenius Kabi Pharmaceutical Company. A population of mice was injected intraperitoneally to give 10 mg drug/kg at ZT20, or 4 h before lights on. After predetermined repair times lasting up to 70 days, mice were euthanized by asphyxiation with CO_2. Liver was isolated, homogenized, and centrifuged as described previously (13). The supernatant obtained by pelleting the chromatin fraction contains the oligonucleotide products of excision repair, and this supernatant (13) was used for our XR-seq analysis. The pellet, which contains the remainder of the genome, was used in this study for slot blot analysis to determine adduct levels. The experiment was repeated with a second population of mice so that all XR-seq data represent results of two independent experiments.

Slot blot

For slot blot analysis, DNA was purified from pellets using the QIAamp DNA Mini Kit (51306), then was mixed with 4 μl RNase A (Sigma, R4642) and incubated for ~1 h at room temperature. Samples were then purified using the QIAquick PCR Purification Kit (28106) and dsDNA concentrations were determined using a Qubit 3.0 Fluorometer. Samples were diluted to 150 ng in 250 μl of 0.1 mM Tris, pH 8.0, heat denatured, cooled quickly in ice water, and mixed with an equal volume of cold ammonium acetate (2.0 M). Samples were then applied to a slot blot apparatus to bind DNA to nitrocellulose (GE Healthcare Hybond ECL RPN303D). Membranes were then baked for 2 h at 80 °C in a vacuum oven, blocked with a solution containing 5% nonfat dried milk, and probed for Pt-d(GpG) adducts with a 1:10000 dilution of antibody from Abcam (ab-103261). Membranes were then stripped for 45 min at room temperature and reprobed with a 1:6000 dilution of antibody from Millipore Sigma (MAB3034) specific for ssDNA, as a control to determine the amount of DNA bound to the membrane. Immunoreactivity was detected using Bio-Rad Clarity reagents to detect horseradish peroxidase–linked secondary antibodies, and images were captured using a Bio-Rad ChemiDoc XRS imaging device and were quantified digitally using ImageJ. Values obtained for amount of cisplatin detected at each time point were corrected using corresponding values obtained for ssDNA detected at each time point to determine ratios of cisplatin/DNA, which are presented.

Sequence and XR-seq data processing

At least 5 million unique mapped reads were obtained for each sample. Analysis of sequencing reads and data visualization were as described previously (13). For plotting average repair profiles as a unit gene, we chose the genes with length >100 kbp and reads per kilobase pairs per million (RPKM) > 0.1 at cisplatin injection times after 2 h. With these criteria, the total number of genes selected was 1418. Each gene was evenly divided into 200 bins from the TSS to the transcription end site (TES), and for each bin, from first to last, an average value for each of the 1418 genes was obtained and plotted. The *y* axis average RPKM for each bin was plotted with *R*.

For genome-level analysis in Fig. 6, we used the annotated genes (based on the UCSC Genome Browser (http://genome.ucsc.edu) (49)).[3] At each time point, reads mapping to the TS of these genes was divided by the total genomic reads to obtain the percent repair in the TS. Percent repair in the remainder of the genome was obtained by subtracting the percent repair in the TS from 100%.

Author contributions—Y. Y. and Z. L. data curation; Y. Y. software; Y. Y. and Z. L. formal analysis; Y. Y., C. P. S., and A. S. writing-original draft; Y. Y., Z. L., C. P. S., and A. S. writing-review and editing; C. P. S. project administration; A. S. funding acquisition; A. S. investigation.

References

1. Partch, C. L., Green, C. B., and Takahashi, J. S. (2014) Molecular architecture of the mammalian circadian clock. *Trends Cell Biol.* **24,** 90–99 CrossRef Medline
2. Kang, T. H., Reardon, J. T., Kemp, M., and Sancar, A. (2009) Circadian oscillation of nucleotide excision repair in mammalian brain. *Proc. Natl. Acad. Sci. U.S.A.* **106,** 2864–2867 CrossRef Medline
3. Gaddameedhi, S., Selby, C. P., Kaufmann, W. K., Smart, R. C., and Sancar, A. (2011) Control of skin cancer by the circadian rhythm. *Proc. Natl. Acad. Sci. U.S.A.* **108,** 18790–18795 CrossRef Medline
4. Sancar, A. (1996) DNA excision repair. *Annu. Rev. Biochem.* **65,** 43–81 CrossRef Medline
5. Wood, R. D. (1997) Nucleotide excision repair in mammalian cells. *J. Biol. Chem.* **272,** 23465–23468 CrossRef Medline
6. Hu, J., Selby, C. P., Adar, S., Adebali, O., and Sancar, A. (2017) Molecular mechanisms and genomic maps of DNA excision repair in *Escherichia coli* and humans. *J. Biol. Chem.* **292,** 15588–15597 CrossRef Medline
7. Hu, J., Adar, S., Selby, C. P., Lieb, J. D., and Sancar, A. (2015) Genome-wide analysis of human global and transcription-coupled excision repair of UV damage at single-nucleotide resolution. *Genes Dev.* **29,** 948–960 CrossRef Medline
8. Hu, J., Lieb, J. D., Sancar, A., and Adar, S. (2016) Cisplatin DNA damage and repair maps of the human genome at single-nucleotide resolution. *Proc. Natl. Acad. Sci. U.S.A.* **113,** 11507–11512 CrossRef Medline
9. Hu, J., Li, W., Adebali, O., Yang, Y., Oztas, O., Selby, C. P., and Sancar, A. (2019) Genome-wide mapping of nucleotide excision repair with XR-seq. *Nat. Protoc.* **14,** 248–282 CrossRef Medline
10. Oztas, O., Selby, C. P., Sancar, A., and Adebali, O. (2018) Genome-wide excision repair in *Arabidopsis* is coupled to transcription and reflects circadian gene expression patterns. *Nat. Commun.* **9,** 1503 CrossRef Medline
11. Li, W., Adebali, O., Yang, Y., Selby, C. P., and Sancar, A. (2018) Single-nucleotide resolution dynamic repair maps of UV damage in *Saccharomy-*

[3] Please note that the JBC is not responsible for the long-term archiving and maintenance of this site or any other third party hosted site.

ces cerevisiae genome. *Proc. Natl. Acad. Sci. U.S.A.* **115,** E3408–E3415 CrossRef Medline
12. Adebali, O., Sancar, A., and Selby, C. P. (2017) Mfd translocase is necessary and sufficient for transcription-coupled repair in *Escherichia coli*. *J. Biol. Chem.* **292,** 18386–18391 CrossRef Medline
13. Yang, Y., Adebali, O., Wu, G., Selby, C. P., Chiou, Y. Y., Rashid, N., Hu, J., Hogenesch, J. B., and Sancar, A. (2018) Cisplatin-DNA adduct repair of transcribed genes is controlled by two circadian programs in mouse tissues. *Proc. Natl. Acad. Sci. U.S.A.* **115,** E4777–E4785 CrossRef Medline
14. Yimit, A., Adebali, O., Sancar, A., and Jiang, Y. (2019) Differential damage and repair of DNA-adducts induced by anti-cancer drug cisplatin across mouse organs. *Nat. Commun.* **10,** 309 CrossRef Medline
15. Hanawalt, P. C., and Spivak, G. (2008) Transcription-coupled DNA repair: Two decades of progress and surprises. *Nat. Rev. Mol. Cell Biol.* **9,** 958–970 CrossRef Medline
16. Menet, J. S., Rodriguez, J., Abruzzi, K. C., and Rosbash, M. (2012) Nascent-Seq reveals novel features of mouse circadian transcriptional regulation. *Elife* **1,** e00011 CrossRef Medline
17. Fang, B., Everett, L. J., Jager, J., Briggs, E., Armour, S. M., Feng, D., Roy, A., Gerhart-Hines, Z., Sun, Z., and Lazar, M. A. (2014) Circadian enhancers coordinate multiple phases of rhythmic gene transcription in vivo. *Cell* **159,** 1140–1152 CrossRef Medline
18. Nojima, T., Gomes, T., Carmo-Fonseca, M., and Proudfoot, N. J. (2016) Mammalian NET-seq analysis defines nascent RNA profiles and associated RNA processing genome-wide. *Nat. Protoc.* **11,** 413–428 CrossRef Medline
19. Wang, D., and Lippard, S. J. (2005) Cellular processing of platinum anticancer drugs. *Nat. Rev. Drug Discov.* **4,** 307–320 CrossRef Medline
20. Kelland, L. (2007) The resurgence of platinum-based cancer chemotherapy. *Nat. Rev. Cancer* **7,** 573–584 CrossRef Medline
21. Hall, M. D., Okabe, M., Shen, D. W., Liang, X. J., and Gottesman, M. M. (2008) The role of cellular accumulation in determining sensitivity to platinum-based chemotherapy. *Annu. Rev. Pharmacol. Toxicol.* **48,** 495–535 CrossRef Medline
22. Chaney, S. G., and Sancar, A. (1996) DNA repair: Enzymatic mechanisms and relevance to drug response. *J. Natl. Cancer Inst.* **88,** 1346–1360 CrossRef Medline
23. Liedert, B., Pluim, D., Schellens, J., and Thomale, J. (2006) Adduct-specific monoclonal antibodies for the measurement of cisplatin-induced DNA lesions in individual cell nuclei. *Nucleic Acids Res.* **34,** e47 CrossRef Medline
24. Veloso, A., Kirkconnell, K. S., Magnuson, B., Biewen, B., Paulsen, M. T., Wilson, T. E., and Ljungman, M. (2014) Rate of elongation by RNA polymerase II is associated with specific gene features and epigenetic modifications. *Genome Res.* **24,** 896–905 CrossRef Medline
25. Andrade-Lima, L. C., Veloso, A., and Ljungman, M. (2015) Transcription blockage leads to new beginnings. *Biomolecules* **5,** 1600–1617 CrossRef Medline
26. Andrade-Lima, L. C., Veloso, A., Paulsen, M. T., Menck, C. F., and Ljungman, M. (2015) DNA repair and recovery of RNA synthesis following exposure to ultraviolet light are delayed in long genes. *Nucleic Acids Res.* **43,** 2744–2756 CrossRef Medline
27. Chiou, Y. Y., Hu, J., Sancar, A., and Selby, C. P. (2018) RNA polymerase II is released from the DNA template during transcription-coupled repair in mammalian cells. *J. Biol. Chem.* **293,** 2476–2486 CrossRef Medline
28. Ljungman, M. (1999) Recovery of RNA synthesis from the DHFR gene following UV-irradiation precedes the removal of photolesions from the transcribed strand. *Carcinogenesis* **20,** 395–399 CrossRef Medline
29. Lavigne, M. D., Konstantopoulos, D., Ntakou-Zamplara, K. Z., Liakos, A., and Fousteri, M. (2017) Global unleashing of transcription elongation waves in response to genotoxic stress restricts somatic mutation rate. *Nat. Commun.* **8,** 2076 CrossRef Medline
30. Bugai, A., Quaresma, A. J. C., Friedel, C. C., Lenasi, T., Duster, R., Sibley, C. R., Fujinaga, K., Kukanja, P., Hennig, T., Blasius, M., Geyer, M., Ule, J., Dolken, L., and Barboric, M. (2019) P-TEFb activation by RBM7 shapes a pro-survival transcriptional response to genotoxic stress. *Mol. Cell* **74,** 254–267.e210 CrossRef Medline
31. Jiang, H., Wolgast, M., Beebe, L. M., and Reese, J. C. (2019) Ccr4-Not maintains genomic integrity by controlling the ubiquitylation and degradation of arrested RNAPII. *Genes Dev.* **33,** 705–717 CrossRef Medline
32. McKay, B. C., Stubbert, L. J., Fowler, C. C., Smith, J. M., Cardamore, R. A., and Spronck, J. C. (2004) Regulation of ultraviolet light-induced gene expression by gene size. *Proc. Natl. Acad. Sci. U.S.A.* **101,** 6582–6586 CrossRef Medline
33. Adar, S., Hu, J., Lieb, J. D., and Sancar, A. (2016) Genome-wide kinetics of DNA excision repair in relation to chromatin state and mutagenesis. *Proc. Natl. Acad. Sci. U.S.A.* **113,** E2124–E2133 CrossRef Medline
34. Tippens, N. D., Vihervaara, A., and Lis, J. T. (2018) Enhancer transcription: What, where, when, and why? *Genes Dev.* **32,** 1–3 CrossRef Medline
35. Vo Ngoc, L., Wang, Y. L., Kassavetis, G. A., and Kadonaga, J. T. (2017) The punctilious RNA polymerase II core promoter. *Genes Dev.* **31,** 1289–1301 CrossRef Medline
36. Sancar, A. (2016) Mechanisms of DNA repair by photolyase and excision nuclease (Nobel Lecture). *Angew Chem. Int. Ed. Engl.* **55,** 8502–8527 CrossRef Medline
37. Sancar, A., Lindsey-Boltz, L. A., Gaddameedhi, S., Selby, C. P., Ye, R., Chiou, Y. Y., Kemp, M. G., Hu, J., Lee, J. H., and Ozturk, N. (2015) Circadian clock, cancer, and chemotherapy. *Biochemistry* **54,** 110–123 CrossRef Medline
38. Fousteri, M., and Mullenders, L. H. (2008) Transcription-coupled nucleotide excision repair in mammalian cells: Molecular mechanisms and biological effects. *Cell Res.* **18,** 73–84 CrossRef Medline
39. Selby, C. P., Drapkin, R., Reinberg, D., and Sancar, A. (1997) RNA polymerase II stalled at a thymine dimer: Footprint and effect on excision repair. *Nucleic Acids Res.* **25,** 787–793 CrossRef Medline
40. Tremeau-Bravard, A., Riedl, T., Egly, J. M., and Dahmus, M. E. (2004) Fate of RNA polymerase II stalled at a cisplatin lesion. *J. Biol. Chem.* **279,** 7751–7759 CrossRef Medline
41. Lainé, J. P., and Egly, J. M. (2006) Initiation of DNA repair mediated by a stalled RNA polymerase IIO. *EMBO J.* **25,** 387–397 CrossRef Medline
42. Brueckner, F., Hennecke, U., Carell, T., and Cramer, P. (2007) CPD damage recognition by transcribing RNA polymerase II. *Science* **315,** 859–862 CrossRef Medline
43. Hara, R., Mo, J., and Sancar, A. (2000) DNA damage in the nucleosome core is refractory to repair by human excision nuclease. *Mol. Cell. Biol.* **20,** 9173–9181 CrossRef Medline
44. Fousteri, M., Vermeulen, W., van Zeeland, A. A., and Mullenders, L. H. (2006) Cockayne syndrome A and B proteins differentially regulate recruitment of chromatin remodeling and repair factors to stalled RNA polymerase II in vivo. *Mol. Cell* **23,** 471–482 CrossRef Medline
45. Anindya, R., Mari, P. O., Kristensen, U., Kool, H., Giglia-Mari, G., Mullenders, L. H., Fousteri, M., Vermeulen, W., Egly, J. M., and Svejstrup, J. Q. (2010) A ubiquitin-binding domain in Cockayne syndrome B required for transcription-coupled nucleotide excision repair. *Mol. Cell* **38,** 637–648 CrossRef Medline
46. Xu, J., Lahiri, I., Wang, W., Wier, A., Cianfrocco, M. A., Chong, J., Hare, A. A., Dervan, P. B., DiMaio, F., Leschziner, A. E., and Wang, D. (2017) Structural basis for the initiation of eukaryotic transcription-coupled DNA repair. *Nature* **551,** 653–657 CrossRef Medline
47. Pines, A., Dijk, M., Makowski, M., Meulenbroek, E. M., Vrouwe, M. G., van der Weegen, Y., Baltissen, M., French, P. J., van Royen, M. E., Luijsterburg, M. S., Mullenders, L. H., Vermeulen, M., Vermeulen, W., Pannu, N. S., and van Attikum, H. (2018) TRiC controls transcription resumption after UV damage by regulating Cockayne syndrome protein A. *Nat. Commun.* **9,** 1040 CrossRef Medline
48. Wilson, M. D., Harreman, M., and Svejstrup, J. Q. (2013) Ubiquitylation and degradation of elongating RNA polymerase II: The last resort. *Biochim. Biophys. Acta* **1829,** 151–157 CrossRef Medline
49. Kent, W. J., Sugnet, C. W., Furey, T. S., Roskin, K. M., Pringle, T. H., Zahler, A. M., and Haussler, D. (2002) The human genome browser at UCSC. *Genome Res.* **12,** 996–1006 CrossRef Medline